

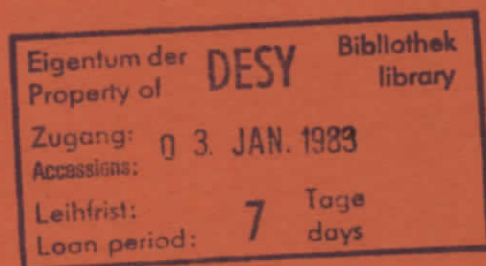
DESY SR 88-05

November 1988

Properties of Synchrotron Radiation and
Instrumentation
for Photoemission and Absorption Spectroscopy

C. Kunz

II. Inst. f. Experimentalphysik, Univ. Hamburg



ISSN 0723-7979

NOTKESTRASSE 85 · 2 HAMBURG 52

DESY behält sich alle Rechte für den Fall der Schutzrechtserteilung und für die wirtschaftliche Verwertung der in diesem Bericht enthaltenen Informationen vor.

DESY reserves all rights for commercial use of information included in this report, especially in case of filing application for or grant of patents.

To be sure that your preprints are promptly included in the
HIGH ENERGY PHYSICS INDEX ,
send them to the following address (if possible by air mail) :

DESY
Bibliothek
Notkestrasse 85
2 Hamburg 52
Germany

Properties of Synchrotron Radiation and Instrumentation
for Photoemission and Absorption Spectroscopy

C. Kunz

II. Institut für Experimentalphysik der Universität Hamburg,

Luruper Chaussee 149, D-2000 Hamburg 50, FRG

Summary

The properties of synchrotron radiation are summarized with a special emphasis on the directions of future developments, namely the planned dedicated storage rings equipped with undulators and wigglers having electron beams with diameters in the 100 μm region. In a second chapter the special instrumentation, especially monochromators, which have to function in combination with high power wigglers and high brilliance undulators, are discussed. The problems which still need to be solved like e.g. power resistivity and high accuracy of mirrors are pointed out. Finally in a separate chapter the possible applications of synchrotron radiation to photoemission microscopy are discussed. In this chapter the different methods and their limitations to generate a microfocus are considered and one special project in progress is exemplified.

Lecture Notes presented at and to be published in Proceedings of:
International School of Physics "Enrico Fermi", Varenna, July 12-22, 1988
"Photoemission and Absorption Spectroscopy of Solids and Interfaces with
Synchrotron Radiation".



1.- Introduction.

The application of synchrotron radiation from electron storage rings to photoemission and absorption spectroscopy of solids and interfaces is one of the most important experimental developments in recent years for characterizing electronic states. In several cases even contributions to the clarification of the geometrical arrangement of atoms were obtained by this technique and more of this is expected to occur in the future.

The spectrum of synchrotron radiation covers a very wide range of photon energies extending from the visible over the vacuum ultraviolet to the soft and hard x-ray regions. Due to the high cross section for photoabsorption at lower photon energies most photoemission investigations up to date use photon energies below 1000 eV photon energy. Terms as "vacuum ultraviolet" (VUV), "soft x-ray" (SX), "extreme ultraviolet" (XUV) are used to characterize this spectral regime, but it should be noted that the boarder line energies are not well defined due to the historical origin of these notations. In addition, in photoemission experiments the necessary resolution in the order of 10 - 100 meV forbids excitation of valence and outer core electrons to too high kinetic energies.

Monochromators for synchrotron radiation (SR) in the energy range up to 1000 eV are almost uniquely based on reflection gratings. Nevertheless, interesting developments occur where new components like e.g. crystals with wide lattice spacing and multilayers penetrate into this energy range. The other interesting frontier is the extension of photoemission spectroscopy to energies above 1000 eV into the x-ray region proper. Synchrotron radiation originally was used only from bending magnets in synchrotrons and storage rings. These machines were built and optimized for high-energy physics. In recent years a rapid development took place in designing storage rings dedicated to synchrotron radiation work. One op-

timization parameter in such a machine is the source size and source divergence, the product of which is closely related to the so-called "electron beam emittance". The other optimization goal is the provision of as many as possible straight sections around the ring which are long enough and especially tailored with respect to the electron optics to accommodate insertion devices. These are wigglers and undulators, sections with alternating magnetic fields where the electron beam is forced on a sinusoidal path. The overall intensity gain is given by the number of bends N in a wiggler while through interference a factor of up to N^2 is gained in peaks of the spectral distribution (undulator effect).

These devices need monochromators with special components in certain places in order to stand e.g. the great power load and in order to take full advantage of the gain in intensity and more specifically in brilliance. Brilliance is the important parameter by which the quality of the new dedicated storage rings and the insertion devices are judged. Brilliance is the number of photons per given band width per unit source size and unit solid angle. With hypothetically perfect optical elements (focusing mirrors etc.) brilliance is an invariant when the radiation is guided from the source through the monochromator onto the sample. Building improved optical elements (or inventing monochromator mountings which make optimum use of technically feasible elements) is another frontier in the field.

The enormous brilliance generated by undulators in dedicated storage rings with very small emittances can be used advantageously in many different ways. Quite obvious are: better spectral resolution, better energy resolution of the emitted photoelectrons, better accuracy through better photon statistics in order to determine small changes in spectra due to

modulation of the sample properties (temperature, laser excitation etc.) or due to oxidation, gas adsorption, interface reactions, surface phase transitions etc. This requires other properties of the new dedicated storage rings which always are taken as granted on paper but practically are fulfilled only to a certain degree, these are: stability, reproducibility of their properties over long periods and reliability. These properties have to be fulfilled by the complete experimental station. A continuous battle needs to be fought there and unfortunately only the defeats are noted and criticized while the victories go without notice. Certainly the users of synchrotron radiation have to learn that they deal with a light source of unprecedented complexity.

In addition to photoemission other secondary processes like photostimulated desorption and fluorescence will also greatly benefit from the increase in intensity on the sample but they are not within the scope of this paper. In this context it should be remembered that absorption spectroscopy is not only performed by transmission measurements on thin samples but can also be done in a photoemission measurement. The total photoelectric yield from a solid sample displays all the features of the absorption coefficient since the yield is proportional to the power absorbed in a thin surface layer of 20 - 50 Å thickness. There is one direction which will profit from higher brightness more than anything else and this is scanning photoabsorption and photoemission with high spatial resolution. The goal is to focus the radiation down to a point on the sample with 0.1 µm diameter or less with Fresnel zone plates or mirrors. Sufficiently high intensities to allow selection of specific electron energies with an electron energy analyzer are required. Alternatively or additionally spin selection would allow the investigation of magnetic domains at the surface of ferromagnetic materials. Such a microprobe should reveal structures in a very easily interpretable way. Element spe-

cific contrast should be obtainable if photon and electron energies could be varied at choice.

The material included in this lecture is selected in such a way that emphasis is given to developments which point to the future. Examples are selected predominantly from projects with which the author himself was connected in one or another way. The past developments in the field of synchrotron radiation are covered in several reviews of which only three are cited here [1-3]. There is also available a very useful collection of equations and data [4]. The instrumentation of synchrotron radiation is regularly presented in a series of conference proceedings [5-17]. A full survey of all new developments is not within the scope of this lecture. It is anyhow difficult since several recent advances will be spared for presentation at the Conference on Synchrotron Radiation Instrumentation, SRI 88 to be held in Tsukuba, Japan, August 29 - September 2, 1988. The results will be published in a special issue of the Review of Scientific Instruments soon thereafter [14].

In the following the material is arranged in three sections. In section 2. the properties of SR are summarized including the main properties of wigglers and undulators. In section 3 the typical standard instrumentation for spectroscopy and an advanced instrument on a wiggler/undulator is presented with the FLIPPER monochromator at the WI undulator at HASYLAB as a specific and operational example. Section 4 finally is devoted to the discussion of the present attempts and directions to obtain as much intensity as possible in a microfocus. This should allow to make photoemission experiments on microscopic samples and would allow a microscopy with element specific contrast.

2.- Properties of synchrotron radiation

2.1 Radiation from bending magnets

The properties of SR can be calculated by applying the methods of classical electrodynamics to relativistic electrons (or positrons) on circular orbits. The dipole characteristic is relativistically distorted in the laboratory frame into a narrow cone according to fig. 1. The width of the cone is in the order of $\gamma^{-1} = 1 - \beta^2$ where βc is the particle velocity, c the velocity of light and β the ratio of the particle energy relative to the electron rest mass energy.

Already Schott [18] treated this problem in connection with classical models of the atom in the beginning of the century, Ivanenko and Pomeranchuk [19], followed by Schwinger [20], were the first who predicted its importance for circular particle accelerators. Now the main equations are derived in standard textbooks, like those of Sommerfeld [21] and Jackson [22].

The properties of SR are listed as follows:

- 1) Continuous spectrum from the infrared to the region of hard x-rays,
- 2) strong collimation in the instantaneous direction of flight (typically 1mrad),
- 3) linear polarization in the plane of the orbit,
- 4) circular polarization in the "wings" above and below the plane of the orbit,
- 5) pronounced time structure, which is a copy of the pulse structure of the electron beam (pulses as short as 100 ps),
- 6) absolute calculability of all the properties of the source, once parameters of the particle beam are given,
- 7) cleanliness and stability (in particular with storage rings) of the source, which, in contrast to gas-discharge sources, exists in an

extremely good vacuum.

The flux of radiation is shown for BESSY I and the planned storage ring BESSY II in fig. 2 [24]. The thus marked curves give the number of photons/sec. in $\Delta\epsilon/\epsilon = 10^{-3}$ or $\Delta\lambda/\lambda = 10^{-3}$ bandwidth in a 1 mrad wide horizontal segment while vertically intensity is fully integrated. ϵ and λ are photon energy and wavelength respectively. The assumed currents $j = 300$ mA (BESSY I) and $j = 100$ mA (BESSY II) explain most of the difference in the low photon energy region. The fall-off at high energies is determined by the characteristic energy ϵ_c (or wavelength λ_c). It depends on the radius of curvature R the magnetic field B and the particle energy E .

The vertical angular spread $\Delta\psi$ (FWHM) of intensity can be approximated as (see e.g. [25])

$$(2.1) \quad \Delta\psi = (2/\gamma) \cdot (\epsilon_c/\epsilon)^{1/3} \quad \text{for } \epsilon \ll \epsilon_c,$$

$$(2.2) \quad \Delta\psi = (2/\gamma) \cdot (\epsilon_c/3\epsilon)^{1/2} \quad \text{for } \epsilon \gg \epsilon_c.$$

Useful equations are:

$$(2.3) \quad B[\text{T}] \cdot R[\text{m}] = 3.34 E[\text{GeV}]$$

$$(2.4) \quad \gamma = 1957 E[\text{GeV}]$$

$$(2.5) \quad \epsilon_c[\text{eV}] = 2218 E^3[\text{GeV}]/R[\text{m}] \\ = 665.1 B[\text{T}]E^2[\text{GeV}]$$

$$(2.6) \quad \lambda_c[\text{\AA}] = 5.59 R[\text{m}]/E^3[\text{GeV}] \\ 18.64/(B[\text{T}]E^2[\text{GeV}])$$

$$(2.7) \quad \epsilon_c[\text{eV}] = 12400/\lambda_c[\text{\AA}]$$

$$(2.8) \quad I[\text{phot}/(\text{s} \cdot \text{mrad} \cdot 0.1\% \text{BW})] = 4.5 \cdot 10^9 R^{1/3}[\text{m}] \epsilon^{1/3}[\text{eV}] j[\text{mA}] \\ \text{for } \epsilon \ll \epsilon_c.$$

The brilliance $\eta(\psi, \epsilon)$ is defined as the number of photons per sec. per 0.1% bandwidth, per unit area A of the source (which is the cross section of the electron beam) and per solid angle. In contrast to many classical sources $\eta(\psi, \epsilon)$ is a very anisotropic quantity. The maximum brilliance in the plane of the orbit is given from eqs. (2.8) and (2.1) by

$$(2.9) \quad \eta(0, \epsilon) \propto j R^{2/3} A^{-1} \epsilon^{2/3} \quad \text{for } \epsilon \ll \epsilon_c.$$

This quantity is plotted for BESSY I and BESSY II in fig. 3. It is easily recognized that the smaller source size A in BESSY II more than compensates for the lower current. The cross section of the electron beam around the orbit (see e.g. [26]) is variable and characterized by two quantities the position (Z) dependent β -functions $\beta_x(Z)$ and $\beta_y(Z)$ and the invariable horizontal and vertical emittances of the storage ring ϵ_x and ϵ_y . With 5% coupling the vertical emittance would be $\epsilon_y = 0.05 \epsilon_x$. For a given storage ring lattice the emittance varies with beam energy like E^2 . Electrostatic and electromagnetic interactions of the particles within the beam will usually lead to an increase of $\epsilon_{x,y}$ with j . The beam sizes (FWHM) are given by $2.35 \sigma_{x,y}$ and are calculated according to

$$(2.10) \quad \sigma_x = \sqrt{\epsilon_x \beta_x(Z)}$$

The beam divergence is given by

$$(2.11) \quad \sigma_x' = \sqrt{\epsilon_x / \beta_x(Z)} \cdot \sqrt{1 + (\beta_x'(Z)^2 / 4)},$$

$\beta'_x(Z)$ is the derivative of $\beta_x(Z)$ with respect to Z . Due to the second square root term $\sigma_x \cdot \sigma_{x'} = \epsilon_x$ holds only at waists or bellies of the "envelope function", where $\beta'(Z) = 0$.

Due to this function and due to another one which is of lesser influence, the dispersion function $D(Z)$, the beam size and divergence can be varied at different positions around the orbit by the designers of storage rings according to the needs of the experiments.

The variation is possible within wide boundaries but the general rule is that σ_x and $\sigma_{x'}$ are coupled through eqs. (2.10) and (2.11) and change in opposite directions. The size of the electron beam determines the source size and its divergence has to be convoluted with the natural divergence of synchrotron radiation. This does not only reduce the brilliance of the source but also mixes the different types of polarization and thereby reduces the actual degrees of polarization.

More information on the design and optimization of storage rings is now available in several reviews [7,9,11].

2.2 Radiation from Wigglers and Undulators

Fig. 4 shows different types of insertion devices [26] for which straight sections with lengths between 2 and 6 m will be provided in the next generation of dedicated storage rings (ALS (Berkeley), Sincrotrone Trieste (Triest), BESSY II (Berlin)). In these machines the electron beam optics is matched at the beginning and end of the straight sections in such a way that additional magnetic lenses (quadrupoles) can shape the β -function at the insertion devices in a large variety of ways without otherwise affecting the storage ring. Variations of the parameters of the insertion devices like e.g. magnetic fields should also be decoupled from the rest of

the storage ring. Up to now these are design goals for which solutions appear to exist in theory, not much practical experience has yet been gained, however.

A wavelength shifter (fig. 4), typically a superconducting magnet at high magnetic field, is a device in which high photon energies are produced in low energy storage rings according to eq. (2.5). Presently such devices are operated at the ADONE ring (Frascati), at the SRS (Daresbury), at the NSLS (Brookhaven), at the PHOTON FACTORY (Tsukuba), at NOVOSIBIRSK (USSR) and elsewhere.

A multipole wiggler deflects the beam to a sinusoidal path in a plane while a helical wiggler generates a spiral path (see fig. 4). They need specially shaped magnetic configurations. In the first case linearly polarized radiation is produced while the helical wiggler produces circular polarization. Circular polarization is of great interest in the investigation of magnetic phenomena and can successfully be combined with electron spin analysis.

A multipole wiggler produces N -times the flux of a bending magnet if the peak magnetic field of the wiggler is the same as that of the bending magnet. More accurately a superposition of contributions from all points on the trajectory has to be calculated and results in a narrow angular distribution around the symmetry line of the wiggler. It turns out, however, to be not just a superposition of intensities but rather of amplitudes which interfere. Although typical period lengths λ_0 of wigglers are macroscopic and are in the order of $\lambda_0 = 2 - 20$ cm the whole structure displays strong interference patterns for wavelengths down to $\lambda = 1 \text{ \AA}$. This undulator effect is explained in fig. 5.

There are three contributions to the phase shift between light and electrons while both travel a period length λ_0 of the wiggler/undulator. The sum of the three path differences l_1 has to fulfil the condition of constructive interference

$$(2.12) \quad l_1 + l_2 + l_3 = m\lambda$$

Due to the small difference of the speed of the electron v to the speed of light c even if both travel on a straight line there is a shift l_1 given by

$$(2.13) \quad l_1 = \frac{c-v}{c} \lambda_0 \approx \frac{1}{2} \left(1 - \left(\frac{v}{c}\right)^2\right) \lambda_0 = \frac{1}{2} \delta^{-2} \lambda_0$$

The second contribution l_2 arises from the detour which the electron makes on its curved path compared to a straight line. This path integral is readily evaluated for a sinusoidal path, it depends of course on the maximum magnetic field, and the electron energy parameter γ .

The result is

$$(2.14) \quad l_2 = \frac{\lambda_0 K^2}{4 \gamma^2}$$

where K is called the undulator parameter

$$(2.15) \quad K = 93.4 B[T] \lambda_0 [m] \\ = \alpha \gamma$$

with α the angle of intersection of the sine wave and the symmetry line (see fig. 5).

If radiation from the undulator is observed from a direction, which is at an angle θ with the symmetry line (this angle may have any azimuth), the typical path length change encountered in observing wave fronts originating from points λ_0 apart is

$$\lambda_0 - l_3 = \lambda_0 \cos \theta \approx \lambda_0 - \frac{\lambda_0}{2} \theta^2$$

This yields

$$(2.16) \quad l_3 = \frac{\lambda_0}{2} \theta^2$$

From eqs. (2.12) to (2.16) we obtain the positions of the interference peaks in the spectrum as

$$(2.17) \quad \lambda_m = \frac{1}{m} \frac{\lambda_0}{2 \gamma^2} \left(1 + \frac{K^2}{2} + \gamma^2 \theta^2\right)$$

Comparing the corresponding undulator peak energies with ϵ_c from eq. (2.5) we obtain

$$(2.18) \quad \frac{\epsilon_m}{\epsilon_c} = 1.33 \frac{m}{K(1 + \frac{K^2}{2})}$$

If ϵ_m/ϵ_c is much larger than 1 there will not be much intensity in the undulator peak. An exact evaluation shows that the maximum intensities in the $m = 1, 3, 5, 7$ harmonics occur for $K = 1.2, 1.9, 2.3, 2.6$ respectively.

The quantitative theory of undulator radiation has been worked out in detail and allows an exact prediction of the properties of a specific design. Many features are already easily derived from the model presented here:

1) There is no intensity in even harmonics along the axis ($\theta=0$). The reason is the antisymmetric emission within one "unit cell". The left wiggler emits radiation with opposite phase to the right wiggler which pro-

vides a N^2 dependence (N is the number of poles!) of the intensity in odd orders but destructive interference for even orders.

2) Defining an in-plane angle ψ and an out-of-plane angle θ perpendicular to the plane of the linear wiggler such that $\theta^2 = \psi^2 + \phi^2$ the antisymmetry of the unit cell mentioned under 1) is broken in the ψ -direction but not in the θ -direction. Even orders will appear only in the ψ -direction.

3) In analogy to other interference phenomena for a specific wavelength λ_m cancellation of intensity occurs if the phase shift of radiation from both ends of the undulator is 2π . For a fixed wavelength λ_m this occurs in analogy to eq. (2.16) at an angle $\theta_0^2 L/2 = \lambda_m$ where L is the length of the undulator. Therefore

$$(2.19) \quad \theta_0 \approx \sqrt{2\lambda_m/L}$$

is roughly the width of the central maximum. For $\lambda_m = 20 \text{ \AA}$ and $L = 4 \text{ m}$ we obtain $\theta_0 \approx 3 \cdot 10^{-5}$ rad, which demonstrates the need of high angular resolution to resolve the angular distribution of an undulator.

4) The same consideration as used in deriving eq. (2.19) at a fixed angle θ yields a minimum in the intensity if $(\lambda - \lambda_m)m \cdot N/2 = \lambda_m$. $\Delta\lambda = \lambda - \lambda_m$. This gives for the width of the undulator lines

$$(2.20) \quad \Delta\lambda/\lambda = 2/(N \cdot m) = \lambda_0/(L \cdot m)$$

This e.g. means that in first ($m=1$) order the relative spectral resolution is the reciprocal of the number of periods.

5) Most of the present day undulator structures are built from periodic

arrangements of permanent magnets, which are glued to two bars mounted (mostly outside the vacuum chamber) on both sides of the electron beam. By varying the wiggler gap also B is varied and thus K. This is the way to tune the undulator harmonics to different wavelengths. In the new storage rings it will be attempted to vary K synchronously with the wavelength scan of the monochromators by microcomputer control. Thus, the tuning to the maximum intensity is always maintained.

6) If the radiation pattern of an undulator is integrated over a wide angular acceptance in ϕ and ρ , or if the angular spread of the electron beam is very large, there is also intensity between the undulator peaks. This is due to the $\gamma^2 \theta^2$ term in eq. (2.18). Nevertheless, sharp structures in the spectrum persist since the θ^2 -shift is always directed to longer wavelengths. Such a spectrum is shown in fig. 6.

7) For the design of the first optical element in a wiggler or undulator beam line the total emitted power is of great importance. This power P is given for wigglers and undulators likewise by

$$(2.21) \quad P[\text{kW}] = 0.633 E^2 [\text{GeV}] B_0^2 [\text{T}] L[\text{m}] j[\text{A}].$$

8) The polarization of an undulator is linear since the circular polarization, which changes from left hand to right hand above and below the orbital plane of a bending magnet, disappears with the simultaneous presence of right-hand and left-hand bends in an undulator. The direction of linear polarization is horizontal in the undulator plane but changes direction outside the plane.

Several attempts have been made to produce circular polarization. I only want to mention one recent idea which was tested already successfully in the visible.

Figure 7 shows the arrangement originally proposed by Onuki [27]. Later a prototype was built and tested [28]. The device consists of a crossed pair of linear undulators AA and BB. The gap of each pair can be tuned from 57 to 146 mm. The relative phase α of the two pairs of magnet structures could be shifted mechanically between $-\pi/2 \leq \alpha \leq +\pi/2$ thus forcing the electron beam into a right-hand and a left-hand spiral at the extremes. With $\alpha=0$ a linear undulator is realized. This undulator produces light with any degree of elliptical polarization. It may well be necessary to produce elliptical degrees of polarization in order to obtain circular polarization at the exit slit of the monochromator. The performance in the visible was in agreement with theory at the 600 MeV storage ring TERAS. The peak magnetic fields were 0.15 T in the helical field configuration and 0.21 T in the plane field configuration. The authors managed to modulate the polarization with a motor drive at a rate of 3 Hz. This arrangement appears to be a promising device.

There are other ideas under discussion for the production of circular polarization. In one case [29] the two perpendicular plane field undulators are placed one behind the other and the phase shift is imposed on the electron beam in a single controllable wiggle between the two undulators. The other idea which is especially considered for wigglers in the hard x-ray regime is to build a device with, say, high field left-hand bends and low field right-hand bends [30]. Of course the field integral as in any other wiggler too has to be zero. Then, in the same way as with bending magnets right- and left-hand elliptic polarization is obtained above and below the wiggler plane for the high energy end of the spectrum.

Finally I want to point out that using a storage ring with a higher beam energy E (or γ) makes the design of wigglers and undulators much simpler. In order to achieve a certain short wavelength λ according to eq. (2.17)

great efforts need to be made if γ is too small. If an undulator optimized for $m=1$ is desired, $K=1.2$ is fixed. As a consequence, λ_0 is determined and then B through eq. (2.15). The reduction in λ_0 requires increased fields B . Looking into the details of undulator design [31] it turns out that the magnet gap needs to decrease proportionally to λ_0 if the field B should be kept constant but the gap needs to decrease faster than λ_0 if the field needs to grow proportional to $1/\lambda_0$. From this requirement there follows a technical limit to the minimum λ_1 and maximum ϵ_1 achievable with a certain storage ring. Flux and brilliance of wigglers ($K \gg 1$) and undulators designed for BESSY II are shown in figs. 2 and 3.

3. Monochromators and experimental stations

3.1 The main advantage of synchrotron radiation, namely its tunability over a very wide range of photon energies, is also the reason of one of its greatest problems in practice. Typically an energy band of 0.1 eV needs to be filtered out of a continuous spectrum 1000 eV - 50.000 eV wide. This is done by diffracting elements, usually optical reflection gratings and crystals. In addition to the wanted radiation in the diffraction peak unwanted radiation from surface scattering and higher order harmonic diffraction penetrates the exit slit of the monochromator. While the problem of scattered radiation is somewhat relieved by using undulators in the first harmonic tunable undulators which are scanned over a wide photon energy range enhance higher harmonics with increasing values of K more than the fundamental peak. In the beginning of experimental work with synchrotron radiation more than 25 years ago the problem of suppressing false light was considered to be so severe that many spectroscopists considered it to be not solvable. This is one of the reasons of the slow acceptance of synchrotron radiation in the community at that time. Even nowadays the problem is far from being solved satisfactorily and in many cases experi-

mentalists are happy to obtain a 90 - 95 % spectral purity with their monochromators. Indeed, in photoemission experiments the electron energy analysis and the tuning of the exciting radiation allow to identify peaks in spite of this spectral impurity. Whenever intensity measurements are required on an absolute basis serious problems arise.

The typical high performance photoemission station at a bending magnet port of one of the present day high performance storage rings like e.g. BESSY in Berlin or the NSLS in Brookhaven consists of one or several combined toroidal grating monochromators (TGMs) providing up to 10^{12} photons/s in the peak of the spectral range in a resolution interval of ≈ 0.2 eV. The spot on the sample is typically 1 mm wide or somewhat less. This spot size is matched to the acceptance of typical electron spectrometers (cylindrical mirror analyzer, spherical mirror analyzer or display type analyzers with wide angle acceptance and multi channel read out).

TGMs scan by rotating a toroidal grating with fixed entrance and exit slits (see fig. 8). They rapidly go out of focus and thus are restricted to a finite energy range. Nonetheless, the simplicity of the mounting, the nearly stigmatic imaging and the moderate requirements of resolution in solid state spectroscopy gave the TGM a wide distribution after the Jobin-Yvon Company succeeded to put grating structures holographically on toroidal surfaces commercially. The first monochromator of this type was built in the late 70's [32] and installed at the ACO storage ring. It is this type of monochromator which has nowadays the widest distribution, but nevertheless appears not to be the instrument to fulfil the requirements at undulator lines in the future. It should be mentioned that there is recent progress with designs using only plane and spherical optical elements [33] and with plane gratings with variable grating constant [34] to design high resolution monochromators which do not suffer from the imperfections

of non-spherical optical elements any longer.

In the following I am not going to give a complete review of all the different monochromator mountings which have been designed and realized in this field, there exist good surveys and reviews in the literature [35-37] I am also not reviewing the different types and arrangements of electron spectrometers which are in existence. These are altogether not typical for work with synchrotron radiation. They could be used or are actually used as well in combination with classical fixed photon energy sources. The rest of this chapter is devoted to the description of the FLIPPER station at the W1 undulator at HASYLAB. In this context those problems which have to be solved for the undulator/wiggler stations at the future dedicated storage rings like the ALS in Berkeley, the Sincrotrone Trieste and the BESSY II in Berlin are exemplified.

3.2 Monochromators at undulators

The FLIPPER monochromator at HASYLAB [38] is a prototype instrument covering almost the full range of interest in this context with the capability of suppressing higher order light by taking advantage of the critical angle of total reflection. As a consequence of this special design the angular acceptance is fairly restricted, which is however no disadvantage in combination with an undulator.

The FLIPPER [39,40] was successfully operated at a bending magnet beamline for almost a decade. Its optical design originates from the GLEISPIMO mounting invented at DESY in 1968 [41,42] and was followed in the meantime by other similar designs, namely the SX 700 at BESSY [43] and the BUMBLEBEE at HASYLAB [44]. Six alternatively used plane mirrors $S_1 \dots S_6$ (see fig. 9) cover the energy range 15 to 450 eV. An additional mirror S_0 which is illuminated at 1.2° grazing angle was added for the set-up at the

wiggler line and covers the energy range up to above 1000 eV. As a matter of fact the Al K edge at 1560 eV can be observed in absorption. There the level of "good" light roughly equals that of stray light. A plane grating (1.5° blaze, 1200 lines/mm) disperses the prefiltered radiation and a paraboloid illuminated at now 2° grazing angle (formerly at 5.7°) focuses a beam of fixed direction into the exit slit. An experimental chamber suitable for photoemission and other surface sensitive techniques is mounted behind the exit slit.

When the installation of a 32-pole wiggler [45] was planned at the 5.3 GeV storage ring DORIS it was decided to split off a VUV beam with a 2.2° grazing incidence mirror alternatively to the x-ray beam. The FLIPPER monochromator with its angular acceptance of roughly 0.2 mrad vertically and 0.8 mrad horizontally almost perfectly matches the emission cone of this special wiggler W1. Furthermore, the undulator peak in first order of the HASYLAB wiggler can be tuned by the gap height over the whole energy range of the FLIPPER monochromator (see table 1).

It is interesting to note that wigglers used in high energy storage rings (from 2 GeV upwards) are not only excellent sources of x-rays but as undulators also deliver more photons in a small solid angle (i.e. more brightness) in the vacuum ultraviolet than wigglers/undulators installed in low energy storage rings. Moreover, much simpler technical solutions are possible and the influence on the storage ring is small. There are, however, some problems involved in using high energy machines like DORIS in the VUV and SX regions which will not exist at smaller machines like e.g. BESSY II.

One of the problems is radiation safety due to the hard x-rays generated by nearby bending magnets in the storage ring tunnel. This problem was

solved at the W1 station by inserting a first plane deflection mirror S_{-1} (see in fig. 9) and by using large beam paths, which are required by the FLIPPER mounting anyhow. There is a long-standing experience at DESY/HASYLAB in coping with such problems.

Another more severe problem was detected only during the continuous operation of this beam-line over the past few years. The W1 wiggler is preceded and followed in the 10 m long straight section by the fringe field of two bending magnets and by several quadrupole magnets which focus the electron beam. A well aligned quadrupole magnet has zero field on axis but the wings of the beam extend already into regions of finite magnetic fields (in the order of 0.01 T). A beam which is not properly aligned, and this may occur frequently in actual storage ring operation, could be subject to even larger fields. From eq. (2.5) it follows that $c_c = 200$ eV at $E = 5.3$ GeV and $B = 0.01$ T. As a consequence a background of not very well controlled radiation is superimposed on the undulator spectrum. With storage rings at lower energy this is not such a severe problem since quadrupoles are operated at magnetic fields gradients proportional to E . As a consequence $\epsilon_c \propto E^3$ and ϵ_c thus decreases rapidly with energy.

A critical element for a successful use of a VUV undulator beam from a high-energy storage ring is the first mirror S_{-1} . It has to take a heat load of up to 600 watt when the wiggler gap is completely closed (see table 1). This power is concentrated in an angular interval of roughly 0.7 mrad horizontally and 0.25 mrad vertically taking into consideration an angular divergence of the electron beam of 0.5×0.07 mrad² (FWHM) at the source point. Due to the grazing angle of 2.2° most of the power is distributed over a strip of 10×100 mm² on the surface.

The mirror itself is a copper block with dimensions $200 \times 50 \times 50$ mm³

covered with Kanigen and polished to high accuracy (90 % of reflected intensity in an angular interval of $\pm 2^\circ = \pm 10 \mu\text{rad}$). It is pressed on a water cooled support with a layer of indium in between providing good thermal contact. The rise in temperature of the mirror block is only some ten degrees measured about halfway between the irradiated surface and the cooled bottom. In order to keep the temperature of this mirror low the Kanigen coating of the backside had to be removed partly for better thermal contact. Without this measure the temperature rose up to 200°C . But even in the new configuration we observe large effects on the intensity of the monochromator output when the wiggler gap is small and thus the power high. We found that these losses originate from mirror S_{-1} . A drop in intensity of up to a factor of two is observed in the first 20 seconds after opening the beam stop. The performance of the monochromator appears to be otherwise unaffected.

From a series of investigations on test mirrors [46] it is understood now that the surface of the mirror reversibly develops a bump due to a large surface temperature decreasing rapidly with a high gradient into the inner of the copper block. Due to the elongated shape of the illuminated part of the surface this bump will act as a cylindrical convex horizontally defocusing mirror which deflects part of the incident radiation in such a way that it is lost at the horizontal apertures. Any additional horizontal divergence added this way to the beam does not pose serious problems to the monochromatization since the spectral resolution of the monochromator depends mainly on vertical imaging. Such distortions of heavily loaded mirrors have been treated theoretically [47,48] (see fig. 10).

It is possible to avoid this effect by operating the wiggler at large gaps. The heat load on the mirror S_{-1} is then drastically reduced. The wiggler still provides a gain of roughly a factor of 40 compared to a

bending magnet. The undulator peak in first order, however, is shifted to 929 eV at 3.7 GeV and $W = 168 \text{ mm}$ (see table 1). With the completely closed gap, $W = 34 \text{ mm}$, the undulator peak is lowered in energy to 36 eV at 3.7 GeV. As will be shown below (see fig. 11), the gain of intensity in the undulator peaks can be appreciable. It can, nevertheless, be advantageous for low photon energies at high currents in the storage ring to sacrifice this option in order to avoid the distortion of mirror S_{-1} and the subsequent losses.

This problem may not be unique to undulators operating at high energy storage rings. In future rings dedicated to the VUV-SX region E will be lower than that of DORIS but tunability over large spectral regions inevitable leads to large values of K which together with the increasing length of undulators will lead to high power loads according to eq. (2.21). Moreover, with the much smaller divergencies of the electron beam the power will be concentrated on a much smaller spot on the surface. The only advantage will be the absence of unwanted hard x-rays. It will become necessary to find ways for better cooling the mirrors, to find materials with high heat conductivity and low thermal expansion [48], and to distribute the heat load over larger areas on the mirror surface by going to larger distances or to apply even shallower angles of incidence for the first mirror in a beam line. The latter measure may well shift the problem to the following elements as was experienced also at the FLIPPER station to some extent.

For 3.7 GeV about 10 % of the radiated power is reflected by mirror S_{-1} . This is incident on mirror S_0 which is made of AlMg_5 coated with Kanigen. This mirror has no water cooling. Due to a large reduction in the apparent aperture a maximum of about 2 % of the total power hits the grating of S_0 is illuminating the grating directly and about 4 % of the total power hits

the mirrors S_1 to S_6 in the other mode. We have detected serious distortions of the mirrors S_1 to S_6 which originally were fabricated from glass (BK7). The heat load resulted in a convex curvature of the flat mirrors probably due to both a bump at the surface and a bending of the whole mirror. This was an especially serious problem for the less grazing incidence mirrors S_3 to S_6 for which most of the incident radiation is also absorbed. The distortion was observed as a defocusing stemming without doubt from these mirrors. It could be partly compensated by changing the focus of the paraboloid. Later on these mirrors were replaced by all-metal mirrors (AlMg₅ covered with Kanigen) and this problem is now solved. Small warm-up effects still occur on S_6 and on the grating which is etched on glass and coated with gold. We have attempted to measure the power incident on S_3 by directly measuring the rise in temperature of this mirror with a thermocouple. The first result, namely 1.5 watt at 5.3 GeV storage ring energy and 30 mA appears to be too low by roughly a factor of 3. A more detailed analysis is needed.

The main information on the performance of the FLIPPER monochromator is condensed in fig. 11. The old bending magnet version was actually operated until August 1984 but no characterisation of the output was made immediately before the transfer to the wiggler line. Therefore the status as of December 82 is given.

The most striking feature is the appearance of the undulator peak in first order and also in higher orders (see ref. [45]). It shifts according to the theoretical calculation given in Table 1. The additional intensity gain in this peak amounts typically to 6. For the common photon energy ranges of the two FLIPPER versions a maximum gain of 200 over the December 82 performance was observed at the undulator. This must not be completely attributed to the undulator since all optical elements and the arrangement of the pre-mirrors have been changed in between.

An analysis of the shape of the undulator peak is given by Grtler [45]. The analysis is based on the solid angle accepted by the FLIPPER optics and yields an excellent agreement between theory and experiment. By deflecting the beam with the help of the remote control of mirror S_{-1} , the sharp undulator peaks decay rapidly as soon as the central ray of the beam is outside of the entrance aperture of the monochromator. This also provides a simple means to align the monochromator to "look head on" to the undulator. It has to be taken into account that the emittance of the electron beam in DORIS and subsequently its angular spread causes a spread of "forward directions". This distribution has the following dimensions at the entrance aperture of the FLIPPER, namely 18 mm horizontally and 2.5 mm vertically (FWHM). This perfectly matches the aperture of the FLIPPER. It becomes obvious from section 2 that the FLIPPER monochromator installed at one of the low emittance storage rings could use smaller apertures without intensity loss in the undulator peak. But it should also be kept in mind that no additional flux would be obtained through the exit slit since all "forward directions" of individual electrons within the beam envelope are collected by the monochromator already now. The real advantage would be an increase in brilliance at the exit slit position, provided perfect monochromator optics is available. Even with present day state of the art quality of aspherical optics brilliance and thereby also spectral resolution could be improved, since the much smaller optical elements could be fabricated with a higher overall accuracy.

Finally, I should mention that the stability of the undulator beam depends very critically on the performance of the storage ring DORIS: If the monochromator is tuned to an undulator peak, very small motions and pulsations of the electron beam become perceptible as intensity fluctuation. A good monitor and good electronics are needed to eliminate this noise from the measurements. Long term drifts change the shape of the whole spectral dis-

tribution and can cause serious troubles depending on the scope of the experiment. Definitely this problem will need to be solved in order to render the new dedicated storage rings useful since they will be much more sensitive due to their smaller emittances.

4.- Microfocusing and microscopy

4.1 General remarks

The general efforts to establish a soft x-ray microscopy with synchrotron radiation are well documented in a series of conference proceedings [49-52]. A microscopy which involves photoelectrons as the signal which generates the image could follow in principle two quite different paths. One method uses an electron optical lens system designed to filter and image photoelectrons within a certain band of kinetic energies with large magnification onto a screen or a two dimensional detector. With the other method a beam of monochromatized synchrotron radiation is focused down to a very small spot which is scanned across the sample. Then photoelectrons of selected energies, or the total emitted flux are providing the signal which generates the image. This type of microscope is already operating in the transmission mode for biological applications at several places [52].

The electron microscopy type of imaging is already in use with an ultraviolet Xenon high power lamp in the first existing LEED-microscope built by Bauer and co-workers [53]. The operation of this microscope in connection with synchrotron radiation involves the incorporation of a filter element. There are also a few other projects of this type e.g. the one by Polack and co-workers in Paris [54] and the one by Bethge and co-workers in Halle [55]. A resolution of 50 Å appears to be achievable. The main challenge for the SR part of this experiment is to maximize radiation density on the object within an area of about 10 µm in diameter.

This is the typical field size for such microscopes. The optical system must be designed and incorporated in such a way that it does not interfere with the electrodes of the electron microscope.

A third type of microscope is only applicable in absorption spectroscopy on thin samples, the direct imaging light microscope. This type of microscopy has been developed by the group Rudolph/Schmahl/Niemann from Göttingen for more than ten years now, see e.g. [49-52]. They use specially designed Fresnel zone plates as lenses and have achieved a resolution in the order of 500 Å. They apply the microscopy exclusively to the investigation of biological objects in the so called water window at 275 eV and at 500 eV photon energy. Additional contrast to the absorption contrast was recently obtained by means of the variations in the real part of the refractive index. This phase contrast needs a specially modified version of the microscope [56].

We turn now again to the scanning microscope which may not match the electron optical microscope with respect to ultimate resolution but in many other respects has advantages over the other types of microscopy. The advantages lie in several places.

- (1) Radiation load on the sample can be minimized compared to the imaging microscope.
- (2) Imaging and electron analysis are well separated measurements.
- (3) Electron spin analysis can be added.
- (4) Other secondary processes, as photostimulated desorption, reflectivity, scattering, can be analysed easily. Absorption can be measured in transmission and by means of the total photoelectric yield.

4.2 Limitations

Fig. 12 shows the general arrangement of a microprobe microscopy station. Starting with an undulator in one of the advanced new planned storage rings radiation originates from a source with an effective source size of roughly 100 μm and a divergence of considerably less than 0.1 mrad. The goal is monochromatization to 0.1 eV unless the natural monochromaticity of undulator radiation of $\Delta\epsilon/\epsilon = 1:50$ is sufficient for certain types of experiments. The further goal is focusing down the radiation to a diffraction limited spot as small as possible. As focusing elements there are available quite generally mirrors with ordinary reflecting coatings, mirrors with specially tailored multilayer coatings, curved crystals and Fresnel zone plates. There are fundamental limitations to the minimum spot size available and technical limitations to the manufacturing of the optical elements. The technical limitations may be overcome step by step due to ingenuity or by investing enough effort and money.

We try now to obtain a rough estimate of the fundamental limitations. The final step of imaging onto the sample must be a large demagnification D of the source itself or of an intermediate image which is defined properly by a diaphragm. According to fig. 13 $D = d/d' = 1/l'$. Then Liouville's theorem (in optics known as the Abbé condition)

$$(4.1) \quad d \sin \theta = d' \sin \theta'$$

provides a relation for the angular widths θ, θ' in the case of perfect imaging. Further, a focus of diameter d requires a minimum angular width due to the coherence condition

$$(4.2) \quad d \sin \theta = \lambda.$$

By d I mean in agreement with the usual definition of the diffraction limit of the classical light microscope the FWHM of the central diffraction peak which is roughly approximated for the purpose of this paper to lie within 20 % of the value given by eq. (4.2).

a) A Fresnel zone plate (see fig. 14) is a circular diffraction grating with the local grating constant Δr determined such that the beam is diffracted to the image point. The grating equation is

$$(4.3) \quad \Delta r(\sin\theta - \sin\theta') = m\lambda$$

where m is the order of diffraction. With small D it follows $\theta' = 0$ and eq. (4.3) reads $\Delta r \sin\theta = m\lambda$. Inserting λ from eq. (4.2) and the local grating constant Δr_{\min} of the outermost zone yields

$$(4.4) \quad d = \Delta r_{\min}/m.$$

If one remembers that all zones must be concentric and spherical to within a fraction of $\Delta r/m$ it is understandable that at present resolution of zone plates is limited to $d \approx 500 \text{ \AA}$. Nevertheless producing zone plates with even lower dimensions of Δr_{\min} appears to be a technical rather than a fundamental limitation. In this context it should be remembered that the "dark" zones need to have a certain thickness t either in order to block the beam or in order to shift the phase of the radiation by $\lambda/2$. The latter is achieved in so called "phase zone plates" taking advantage of the very small deviation of the real part of the index of refraction of 1 in the 500 - 1000 eV range. The aspect ratio $2t/\Delta r_{\min}$, however, becomes forbiddingly large with decreasing Δr_{\min} .

b) Under the assumption that a single mirror constitutes the optical element in the final demagnification stage we come to an estimate for the grazing incidence region (photon energies above 100 eV). From a Drude model for the index of refraction $n = 1 - \omega_p^2 / (2\omega^2) = 1 - \lambda^2 / (2\lambda_p^2)$ with ω_p , λ_p being a plasma frequency and plasma "wavelength" respectively. θ_c the grazing critical angle of total reflection is defined by $n = \cos \theta_c$. θ_c is roughly the angle at which the reflectivity is 50 %. $n \approx 1 - \frac{1}{2} \frac{\lambda^2}{\lambda_p^2}$ for small θ_c yields $\theta_c \approx \lambda / \lambda_p$ and with $\theta = 2 \theta_c$ (see fig. 14) in combination with eq. (4.2).

$$(4.5) \quad d \approx \lambda_p / 2.$$

This effective plasma wavelength of course gives only a rough representation of the optical constants in a certain spectral range. In principle λ_p should be inversely proportional to the square root of the number of "free" electrons per unit volume. In addition to the conduction electrons all those core electrons should be counted which can be excited at a given photon energy and which have exhausted their oscillator strength. Therefore λ_p might decrease slowly with decreasing wavelength. In practice, however, reflectivities are well represented by a constant λ_p , which is e.g. for gold coated mirrors $\lambda_p \approx 200 \text{ \AA}$ over a wide energy range [57]. Taking this λ_p into eq. (4.5) gives an ultimate limit to the obtainable spot size of $d = 100 \text{ \AA}$ with a single mirror optics. With a double mirror optics, e.g. the Wolter type I arrangement [58-59] the limit could become half this value. Other limitations lie of course in the aberrations and in the manufacturing accuracy of mirror elements with complicated shapes.

c) Bent crystal optics and multilayer coated reflecting optics are limited to fixed photon energies but with those elements grazing reflection angles

can be made large. There is, however, the problem that the grazing angle of reflection θ and the wavelength λ are linked by Bragg's law.

$$(4.6) \quad 2d_1 \sin \theta = m\lambda$$

where d_1 is the lattice or multilayer spacing and m the order. Laterally graded lattice constants may be generated with multilayer coatings but not so easily with crystals. A near normal incidence optics like the Schwarzschild arrangement [60] see fig. 15. is probably the optimum for such elements. Due to the large roughness scattering at normal incidence by surface roughness there is a serious technical problem in this arrangement (see eq. (4.9) below).

Normal incidence will also minimize another limitation of such optics which is due to the finite depth in which radiation is reflected (see fig. 14). If l_e is the extinction length the width of the focus due to this effect is

$$(4.7) \quad d = l_e \frac{\sin \theta}{\cos 2\theta}.$$

Since l_e can be in the order of 5000 \AA this effect can seriously influence the size of the focal spot unless θ is less than a few degrees, or unless θ is equal to 90° within a few degrees (back reflection).

d) The simplest way to obtain a microfocus is by placing a pin hole in a parallel beam. The size of the light spot depends on the distance x between the pin hole of diameter d_0 and the sample. Then the size of the spot is given (see fig. 16) as:

$$(4.8) \quad d = d' + 2x \tan \theta + x(\lambda/d')$$

size divergence diffraction

We assume $x = 5 \text{ nm}$, a distance barely large enough in order to be able to extract the photoelectrons from the sample surface. At $\lambda = 20 \text{ \AA}$, neglecting the divergency term, the optimum pin hole size is then $d' = 3 \text{ }\mu\text{m}$ yielding a spot size of $d = 6 \text{ }\mu\text{m}$. The divergency of the beam illuminating the pin hole would have to be $\theta \leq 10^{-4} \text{ rad}$. This amounts, however, to a demagnification $D = 1$ of the undulator source onto the pin hole. The loss of intensity with an assumed source diameter of $100 \text{ }\mu\text{m}$ corresponds to $(3 \text{ }\mu\text{m}/100 \text{ }\mu\text{m})^2 = 10^{-3}$. All this is just a simple demonstration of where the limitations for this simplest possible approach to spatially resolved photoemission lies. Nevertheless, in certain cases, e.g. photoemission on crystals which can only be grown in sizes up to $10 \text{ }\mu\text{m}$, this approach might make sense. Also with photon excited Auger analysis [61] which does not require monochromatization of the exciting radiation such an approach might be reasonable.

Let us finally consider emittance/acceptance matching between the source in the storage ring and the spot on the sample. If the source size of $100 \text{ }\mu\text{m}$ is demagnified by $D = 10^{-3}$ to a spot of 1000 \AA the overall emission angle (electron beam divergence convoluted with the undulator angular distribution) which we assumed as $2\theta = 10^{-4} \text{ rad}$ transforms according to eq. (4.1) by a factor D^{-1} to $2\theta = 10^{-1} \text{ rad}$. This amounts to an angle $\theta = 3^\circ$ or a grazing incidence reflection angle $\theta/2 = 1.5^\circ$. At $\lambda = 10 \text{ \AA}$ $\theta_c = \lambda/\lambda_p = 3^\circ$ for a Au coating is well above this angle. Even further demagnification is feasible without more loss of intensity than that due to the limited reflectivity of the optical elements. One important factor in this context is the loss of specular reflectivity due to roughness. The actual reflectivity is calculated in the simplest theoretical approach from the reflectivity of a perfectly smooth surface R_o by

$$(4.9) \quad R = R_o \exp(-[(4\sigma\cos\theta/2)/\lambda]^2)$$

where σ is the mean square roughness with Gaussian light distribution. The scattered intensity is unfortunately not lost but generates a spread out background in the image of the sample which will reduce the contrast [62].

4.3 A ring mirror microscope

It can easily be shown that a rotationally symmetric (ring shaped) single mirror has two fundamental problems. The most serious one is that such a mirror cannot image an extended area point by point onto another area. Wolter has therefore designed arrangements involving two consecutive reflections which avoid this problem [57,58]. With a small enough segment of a single mirror, however, imaging is feasible with a certain degree of accuracy. The second problem is due to the demagnification D which is not constant for rays reflected at different points in the axial direction along the mirror. This effect limits the usable length w of such mirrors since $\Delta D/D = w/l$, where l is the distance to the image plane. In arrangements where only light is concentrated into a small spot $\Delta D/D = 0.3$ is still acceptable.

The simplest possible rotationally symmetric focusing element is a rotational ellipsoid which collects radiation originating from one focal spot into the other one. Fig. 17 shows an arrangement which is presently set up at the HASYLAB laboratory by the University of Hamburg [63]. The elliptical ring mirror has a diameter of 5 mm , a length of 6 mm and distances $l' = 1000 \text{ mm}$, $l = 35 \text{ mm}$, a demagnification $D = 1 : 30$, a grazing angle of reflection $\theta/2 = 2^\circ$. It will reflect radiation up to $\epsilon = 2000 \text{ eV}$. The imaging properties are such that a point in the object plane at a distance d' from the axis generates a whole circle with a radius $d = Dd'$ in the image plane. This circle is concentric to the axis of the ellipsoid. Thus a con-

centric circle in the image plane is imaged on a concentric demagnified circle in the object plane and a concentric diaphragm of diameter d' has an image of diameter $d = Dd'$. For the purpose of forming a microfocussing mirror fulfils all the necessary requirements. Also calculations involving diffraction show that the diffraction pattern is close, although not exactly equal, to that of an annular aperture of 5 mm diameter and 200 μm width. Therefore the general considerations made above for the resolution limit due to diffraction apply. As a matter of fact due to the necessary apodization eq. (4.2) needs to be modified for a hollow cone yielding approximately

$$(4.10) \quad 2d \sin\theta = \lambda,$$

As a consequence also eq. (4.5) is modified to

$$(4.11) \quad d \approx \lambda_p / 4.$$

In the case of the ellipsoid microscope, with $\theta/2 = 0.035$, $\theta/2 < \theta_c$ for photon energies below 2000 eV.

The hollow cone diffraction pattern is insofar disadvantageous that the central diffraction peak although very prominent contains only about 15% of the total intensity. The rest is smeared out into the diffraction rings of higher order and will generate a background in the image. With the phase I microscope which is presently installed at HASYLAB a 10 μm diameter diaphragm will be demagnified to a $d = 0.33 \mu\text{m}$ diameter image. Because of the imperfections of this first mirror (manufactured by the Zeiss company with the best presently available technology) the final spot size is expected to be in the order of 0.5-1 μm . This has to be compared with the diffraction limit according to eq. (4.10) with $\theta = 0.07$ yielding at $\lambda = 20 \text{ \AA}$

$d = 0.007 \mu\text{m}$. Thus in this phase of the project there is no limitation to be expected due to diffraction. In a phase II which aims at a focus of 0.1 μm this mirror will reach the diffraction limit of 0.1 μm at $\lambda = 300 \text{ \AA}$ corresponding to $\epsilon = 40 \text{ eV}$.

This microscope will be installed behind the FLIPPER station (see section 3.2) at the W1 undulator at HASYLAB. It can be operated with one single alignment in the whole range $\epsilon = 15-1500 \text{ eV}$, its angular acceptance is matched to that of the FLIPPER. The overall intensity loss is: at the exit slit of the monochromator a factor of 10^{-3} (10 μm diaphragm, $300 \times 250 \mu\text{m}^2$ spot size), at the mirror a geometrical acceptance factor of $1.25 \cdot 10^{-2}$. The specular reflectivity of the mirror will depend on its roughness. Some initial tests on prototype mirrors were promising. Assuming an optimistic value of $R = 0.8$ we obtain a general loss factor of 10^{-5} by which the values given in fig. 11 need to be multiplied. At the oxygen K-edge (534 eV) approximately 10^7 photons are expected in the phase I microscope.

Possible gains in intensity at storage rings of lower emittances with monochromators equipped with better optical elements are roughly estimated: A factor of 10 at the entrance aperture, a factor of 5 with a smaller horizontal divergence and a factor of 20 using longer undulators with more periods (conservative estimate). Thus three orders magnitude in the gain appear to be a reasonable estimate due to improvements of the storage rings. Using somewhat longer mirrors or mirrors with higher angles $\theta/2$ could also gain some intensity but to a lesser extent. It should, however, be mentioned that using such a small angle as $\theta/2 = 2^\circ$ also for longer wavelengths enhances specular reflection and reduces roughness scattering according to eq. (4.9).

The mechanical installation is presently under construction in Hamburg. The most important factor is mechanical stability with respect to the axis of the ellipsoid and the scanning of the sample. Not much can be said about this set up before the microscope is thoroughly tested.

Acknowledgement

I want to thank Dipl.Phys. Stefan Cramm and Dipl.Phys. Joachim Voss for a critical reading of the manuscript and Astrid Schmidt for her careful work in preparing the manuscript.

References

- 1 E.E. Koch, Ed: Handbook on Synchrotron Radiation (North Holland, Amsterdam, New York, Oxford, 1983) Vol. 1a,1b,2
- 2 C. Kunz, Ed: Synchrotron Radiation - Techniques and Applications (Springer, Berlin, Heidelberg, New York, 1979) Topics in Current Physics, Vol. 10
- 3 H. Winick and S. Doniach, Eds: Synchrotron Radiation Research (Plenum Press, New York, London, 1980)
- 4 D. Vaughan, ed: X-Ray Data Booklet, Lawrence Berkeley Laboratory, Berkeley, 1986)
- 5 F. Wuilleumier and Y. Farge, Eds: Proceedings of the International Conference on Synchrotron Radiation Instrumentation and New Developments (Orsay, 12-14 Sept. 1977) Nuclear Instrum. Meth. 152 (1978)
- 6 D.L. Ederer, J.B. West, Eds: Proceedings of the National Conference on Synchrotron Radiation Instrumentation (Gaithersburg, 4-6 June 1979) Nuclear Instrum. Meth. 172 (1980)
- 7 M.R. Howells, Ed: Proceedings of the Japanese/USA Seminar on Synchrotron Radiation Facilities (Honolulu, 5-9 Nov. 1979) Nucl. Instrum. Meth. 177 (1980)
- 8 D.M. Mills, B.W. Batterman, Eds: Proceedings of the Second National Conference on Synchrotron Radiation Instrumentation (Ithaca 15-17 July 1981) Nucl. Instrum. Meth. 195 (1982)

- 9 E.E. Koch, Ed: Proceedings of the International Conference on X-Ray and VUV Synchrotron Radiation Instrumentation (Hamburg, 9-13 Aug. 1982) Nucl. Instrum. Meth. 208 (1983)
- 10 W. Thomlinson, G.P. Williams, Eds: Proceedings of the Third National Conference on Synchrotron Radiation Instrumentation (Upton, 12-14 Sept. 1983) Nucl. Instrum. Meth. 222 (1984)
- 11 G.S. Brown, I. Lindau, Eds: Proceedings of the International Conference on X-Ray and VUV Synchrotron Radiation Instrumentation (Stanford, 29 July - 2 Aug. 1985) Nucl. Instrum. Meth. A246 (1986)
- 12 G.N. Kulipanov, Ed: Proceedings of the Seventh USSR National Conference on Synchrotron Radiation Utilization (SR86) (Novosibirsk, 3-5 June 1986) Nucl. Instrum. Meth. A261 (1987)
- 13 M.A. Green, J.P. Stott, P.R. Woodruff, Eds: Proceedings of the Fifth* National Conference on Synchrotron Radiation Instrumentation (Madison 21-25 June 1987) Nucl. Instrum. Meth. A266 (1988) (*actually the "Fourth"!)
- 14 Proceedings of the 3rd International Conference on Synchrotron Radiation Instrumentation: SRI-88 (Tsukuba 29 Aug. - 2 Sept. 1988) Rev. Sci. Instrum., to be published
- 15 M.R. Howells, Ed: Reflecting Optics for Synchrotron Radiation (Conf. Upton 16-18 Nov. 1981) Proc. SPIE 315 (1981)
- 16 E. Spiller, Ed: High Resolution Soft X-Ray Optics (Conf. Brookhaven 18-20 Nov. 1981) Proc. SPIE 316 (1981)

- 17 E.E. Koch, G. Schmahl, Eds: Soft X-Rays Optics and Technology (Conf. Berlin 8-11 Dec. 1986) Proc. SPIE 733 (1986)
- 18 G.A. Schott: Electromagnetic Radiation (Cambridge University Press, Cambridge 1912)
- 19 D. Ivanenko, J. Pomeranchuk: Phys. Rev. 65, 343 (1944)
- 20 J. Schwinger: Phys. Rev. 70, 798 (1946); Phys. Rev. 75, 1912 (1949)
- 21 A. Sommerfeld: Elektrodynamik (Akademische Verlagsgesellschaft, Leipzig 1949)
- 22 J.D. Jackson: Classical Electrodynamics (Wiley and Sons, New York 1962) p. 481 ff.
- 23 D.H. Tomboulian, P.L. Hartman: Phys. Rev. 102, 1423 (1956)
- 24 Proposal: BESSY II, Eine optimierte Undulator/Wiggler-Speicherring Lichtquelle für den VUV- und XUV-Spektralbereich (Berliner Elektronenspeicherring-Gesellschaft für Synchrotronstrahlung mbH, Nov. 1986)
- 25 C. Kunz: in Ref. 2 p. 1
- 26 S. Krinsky, M.L. Perlman, R.E. Watson: in Ref. 1, Vol. 1a, p. 65
- 27 H. Onuki: in Ref. 11, p. 94
- 28 H. Onuki, N. Saito, T. Saito: Appl. Phys. Lett. 52, 173 (1988)

- 29 K.J. Kim: Nucl. Instrum. Meth. 219, 425 (1984)
- 30 J. Goulon, P. Elleaume, D. Raux: Nucl. Instr. Meth. A254, 192 (1987)
- 31 G. Brown, K. Halbach, J. Harris, H. Winick: in Ref. 9, p. 65
- 32 C. Depautex, P. Thiry, R. Pinchaux, Y. Petroff, D. Lepère, G. Passereau, J. Flammand: in Ref. 5, p. 101
- 33 C.T. Chen: Nucl. Instrum. Meth. Phys.Res. A256, 595 (1987)
- 34 T. Harada, T. Kita, M. Itou, H. Taira, A. Mikuni: in Ref. 11, p. 272
- 35 W. Gudat, C. Kunz: in Ref. 2, p. 55
- 36 R.L. Johnson: in Ref. 1, p. 173
- 37 V. Saile, J.B. West: in Ref. 9, p. 199
- 38 F. Senf, K. Berens v. Rautenfeldt, S. Cramm, J. Lamp, J. Schmidt-May, J. Voss, C. Kunz, V. Saile: in Ref. 11, p. 314
- 39 W. Eberhardt, G. Kalkoffen, C. Kunz: in Ref. 5, p. 81
- 40 J. Barth, F. Gerken, C. Kunz, J. Schmidt-May: in Ref. 9, p. 307
- 41 C. Kunz, R. Haensel, B. Sonntag: J. Opt. Soc. Am. 58, 1415 (1968)
- 42 H. Dietrich, C. Kunz: Rev. Sc. Instr. 43, 434 (1972)
- 43 H. Petersen, H. Baumgärtel: in Ref. 6, p. 191

- 44 W. Jark, C. Kunz: in Ref. 11, p. 320
- 45 P. Gürtler: in Ref. 11, p. 91
- 46 S. Mourikis, E.E. Koch, V. Saile: Nucl. Instrum. Meth. A267, 218 (1988)
- 47 R.T. Avery: in Ref. 10, p. 146
- 48 T. Ohta, T. Fujikawa: KEK Report 81-10 (Aug. 1981)
- 49 D.F. Parsons, Ed: Ultrashort X-Ray Microscopy: Its Application to Biological and Physical Sciences (New York 13-15 June 1979) Annals of the New York Academy of Sciences, Vol. 342 (1980)
- 50 G. Schmahl, D. Rudolph, Eds: Proceedings of the International Symposium, X-Ray Microscopy (Göttingen, 14-16 Sept. 1983) Springer Series in Optical Sciences 43 (Springer, Berlin, Heidelberg 1984)
- 51 Ping-chin Cheng, Gwo-jen Jan, Eds: X-Ray Microscopy - Instrumentation and Biological Applications (Proceedings Symposium, Taipei Aug. 1986) (Springer, Berlin, Heidelberg 1987)
- 52 D. Sayre, M. Howells, J. Kirz, H. Rarback, Eds: Proceedings of the International Symposium, X-Ray Microscopy II (Brookhaven 31 Aug. - 4 Sept. 1987) Springer Series in Optical Sciences 56 (Springer Berlin, Heidelberg 1988)
- 53 W. Telieps, E. Bauer: Ultramicroscopy 17, 57 (1985)
- 54 F. Polack, S. Lowenthal, D. Phalippou, P. Fournet: in Ref. 52, p. 220

- 55 H. Bethge, T. Krajewski, O. Lichtenberger: *Ultramicroscopy* 17, 21 (1985)
- 56 G. Schmahl, D. Rudolph, P. Guthmann: in Ref. 52, p. 228
- 57 B.L. Henke, P. Lee, T.J. Tanaka, R.L. Shimabukuro, B.K. Fujikawa:
Atomic Data and Nuclear Data Tables 27, 123 (1982)
- 58 M. Wolter: *Ann. Phys.* 10, 94 (1952);

M. Wolter: *Ann. Phys.* 10, 286 (1952)
- 59 A. Franks, B. Gale: in Ref. 50, p. 129
- 60 R.P. Haelbich, W. Staehr, C. Kunz: in Ref. 49, p. 148
- 61 E. Umbach, Z. Hussain: *Phys. Rev. Lett.* 52, 457 (1984) and private communication
- 62 H. Högrefe, C. Kunz: *Appl. Optics* 26, 2851 (1987)
- 63 C. Kunz, A. Moewes, G. Roy, H. Sievers, J. Voss, H. Wongel: in HASYLAB
Jahresbericht 1987, p. 366, and to be published

Table 1

Parameters of the HASYLAB wiggler/undulator W1. Gap = W, maximum field on orbit = B, photon energy of first order undulator radiation = $h\nu_1$, total emitted powder = P.

Gap W (mm)	B (Tesla)	K			3.7 GeV	5.3 GeV
			3.7 GeV $h\nu_1$ (eV)	5.3 GeV $h\nu_1$ (eV)	100 mA P(Watt)	50 mA P(Watt)
33.8	0.567	7.10	36.2	74.3	609	625
40.0	0.493	6.08	48.7	99.9	446	458
50.0	0.382	4.71	78.5	161	268	275
60.0	0.295	3.64	124	254	160	164
70.0	0.229	2.82	191	392	96	99
80.0	0.176	2.17	283	581	57	59
90.0	0.137	1.69	391	802	35	36
100	0.104	1.28	522	1071	20	21
120	0.063	0.777	729	1496	7.3	8
140	0.036	0.444	864	1773	2.4	2.5
160	0.022	0.271	916	1880	0.9	0.9
168	0.017	0.210	929	1906	0.5	0.6

Figure Captions

- Fig. 1 Angular distribution of synchrotron radiation (a) as emitted in the rest frame of the electron (b) as emitted in the laboratory frame. (From ref. 23)
- Fig. 2 Flux of photons emitted from the bending magnets of BESSY I (300 mA) and II (100 mA) and from the planned wigglers W and U of BESSY II. (From ref. 24)
- Fig. 3 Brilliance of the same elements as in fig. 2. (From ref. 24)
- Fig. 4 Three different types of insertion devices. (From ref. 25)
- Fig. 5 The undulator with period length λ_0 shown in a) fulfils the undulator condition whenever the sum of the three path length differences l_1 , l_2 and l_3 explained in b)-d) is equal to a multiple of the photon wavelength λ . The angle α is relevant in eq. (2.15)
- Fig. 6 Undulator spectra integrated over all angles for different values of the undulator parameter K. (From ref. 26)

- Fig. 7 Undulator design for an undulator with variable left-hand/right-hand circular/elliptic polarization of any degree. The two sets of magnets AA and BB can be shifted with respect to each other by one period, the whole unit can be rotated around the beam. (From ref. 28)
- Fig. 8 Layout of a toroidal grating monochromator with two interchangeable gratings TG(A1), TG(A2). FM are focusing mirrors. (From ref. 33)
- Fig. 9 Layout of the order sorting FLIPPER monochromator at HASYLAB. The mirror S_{-1} can be inserted into the white beam which otherwise serves an x-ray wiggler station. The grating G is either illuminated directly by mirror S_0 or by one of the mirrors $S_1 - S_6$. The paraboloid P focuses monochromatic radiation into the exit slit ES. (From ref. 38). The scale at the bottom gives distances from the source in m
- Fig. 10 Calculated surface deformation by illuminating a copper and a quartz mirror with a wiggler beam at 2° grazing incidence. (From ref. 48)
- Fig. 11 The output of the FLIPPER monochromator of fig. 9 with a maximum 200 μm slit width at a bending magnet (Dec. 82) and at the HASYLAB wiggler/undulator W1 (Dec. 84). The resolution ΔE as given is that for a 200 μm slit and can be reduced by a factor of roughly 1/3 by closing the slit. (From ref 38)

Fig. 12 Typical layout and parameters of a microfocus arrangement at an undulator in one of the next generation storage rings

Fig. 13 Illustration to explain Liouville's theorem in a microfocus arrangement, S = source, I = image, d' and d are corresponding elements of S and I respectively

Fig. 14 Limitations to the smallest spot size d attainable in a microfocus arrangement a) with a Fresnel zone plate with outermost zone separation Δr , b) with mirror optics with the critical angle of total reflection θ_c , c) with a bent crystal with the extinction length l_e contributing to the spot size d , θ is the Bragg angle

Fig. 15 Prototype of a scanning microscope installed at the original DESY synchrotron using a multi-layer coated Schwarzschild objective (From ref. 60)

Fig. 16 Definition of the parameters of a pin hole scanning microprobe

Fig. 17 Principle and parameters of the scanning photoelectron microscope under construction at HASYLAB. F_1, F_2 are the foci of the elliptical mirror

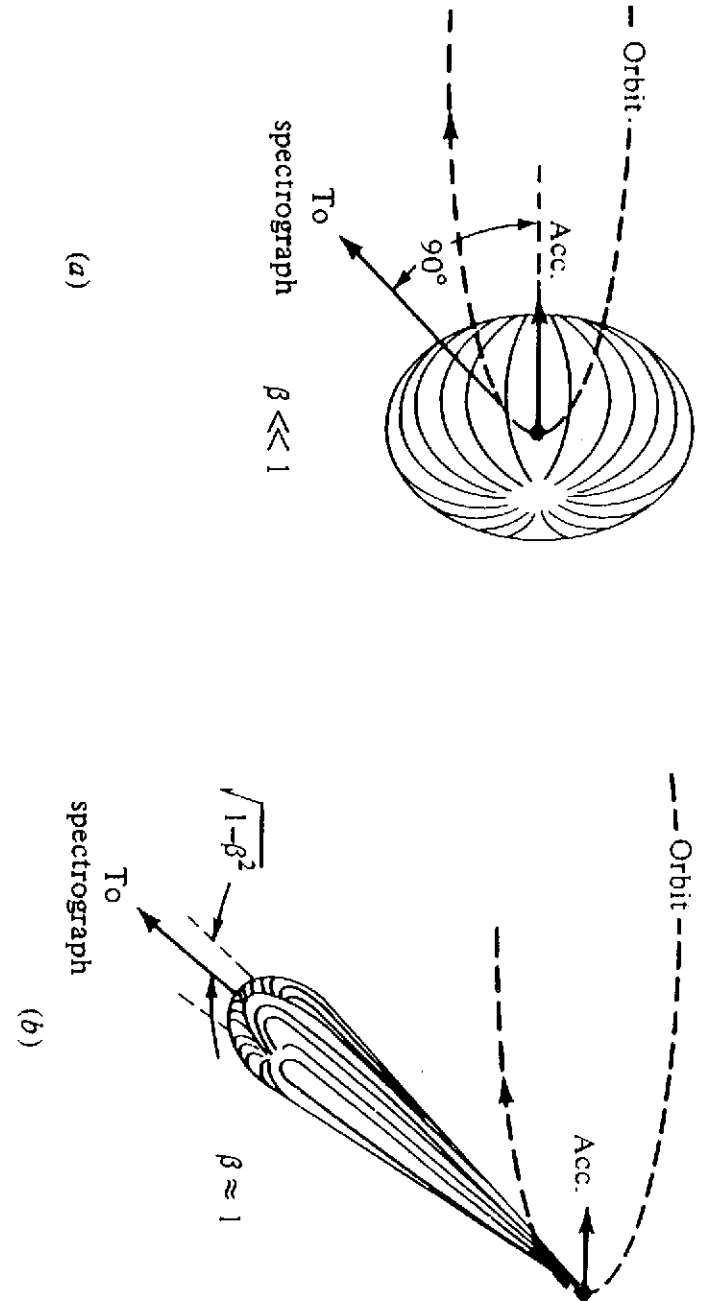


Fig. 1

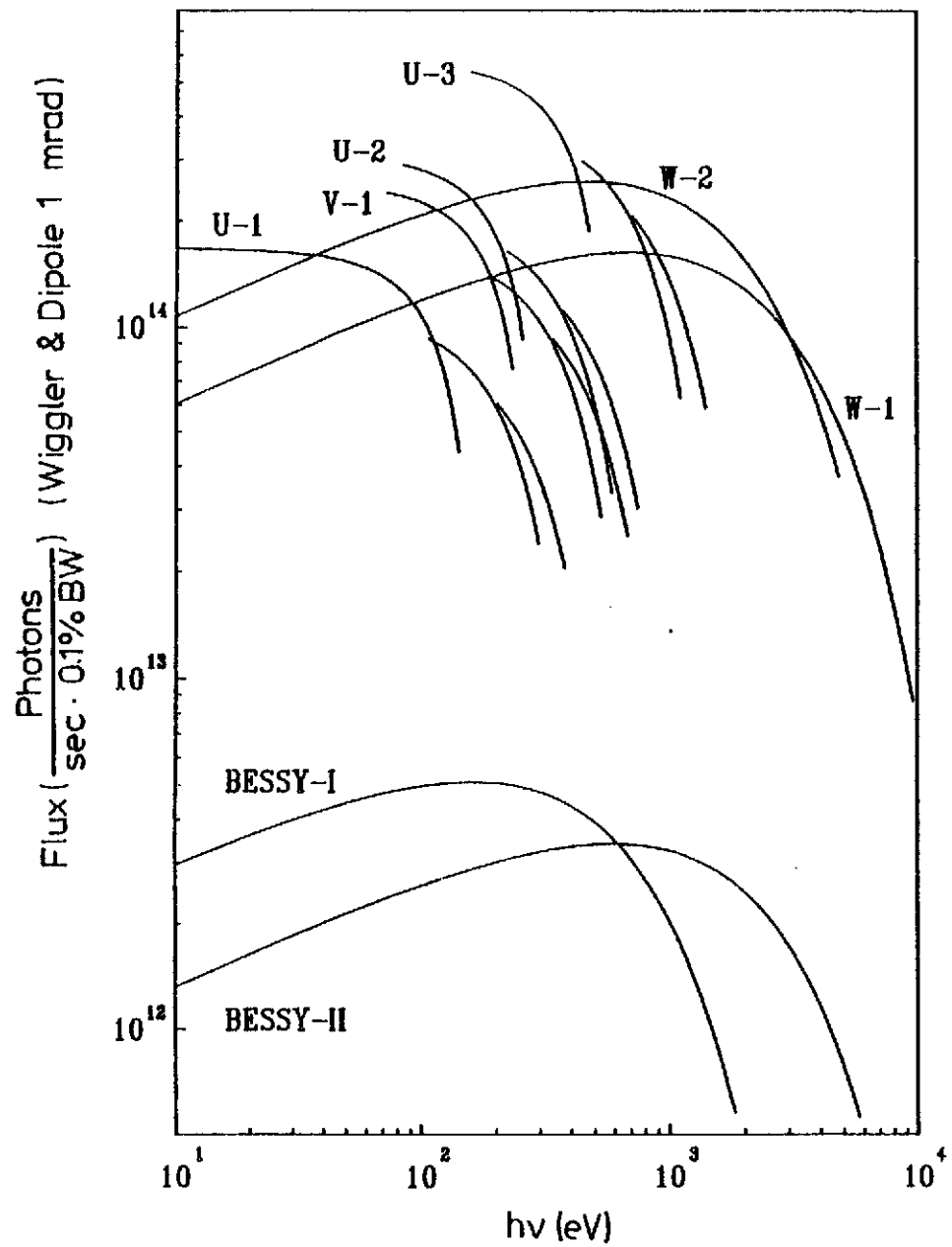


Fig. 2

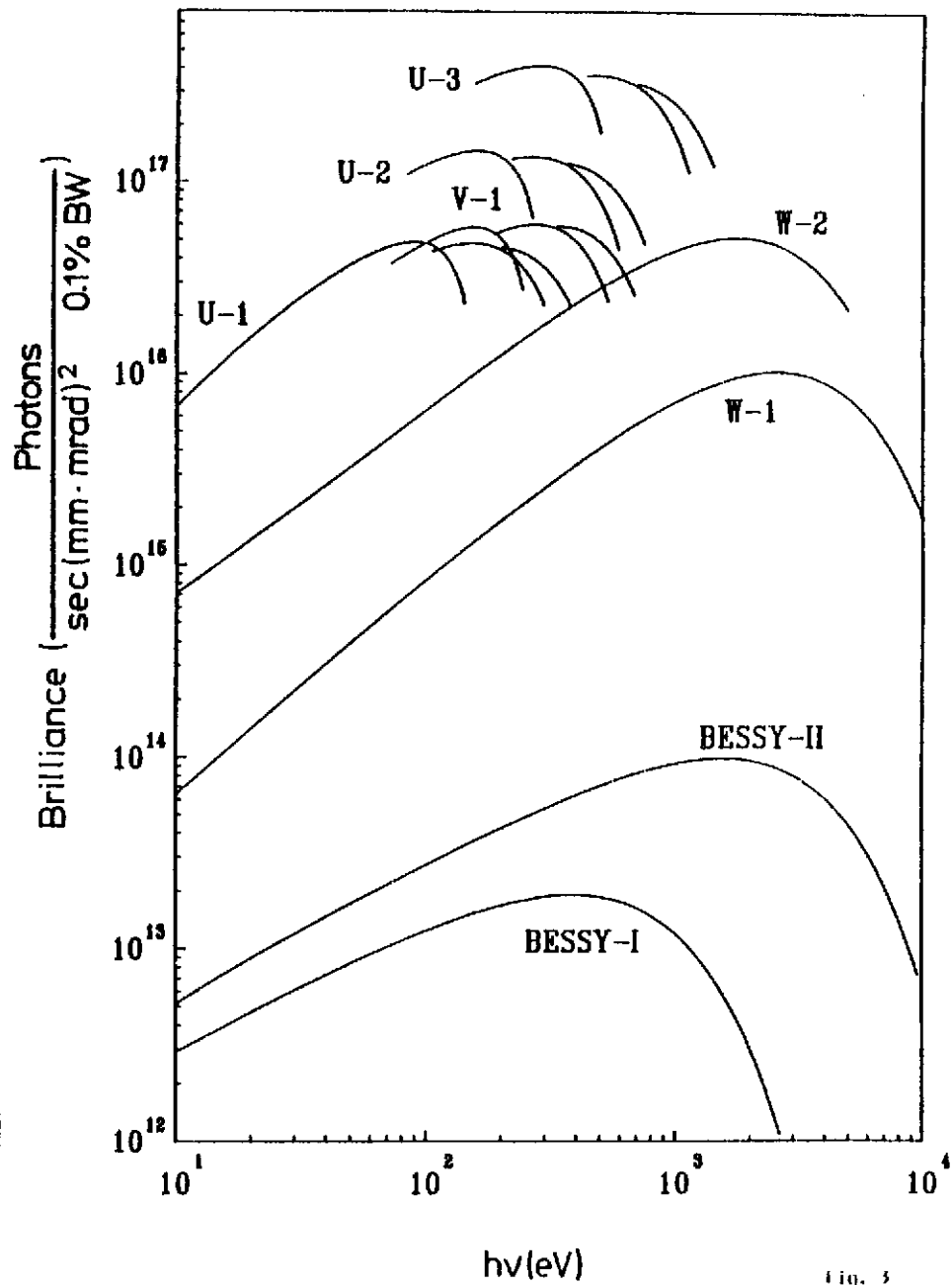
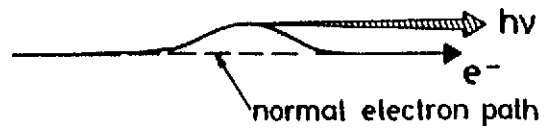
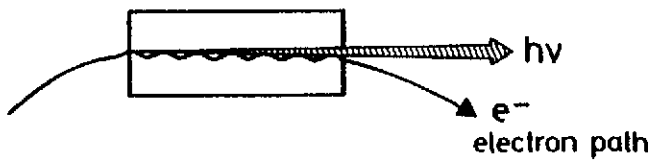


Fig. 3

WAVELENGTH SHIFTER



MULTIPOLE WIGGLER MAGNET



HELICAL WIGGLER

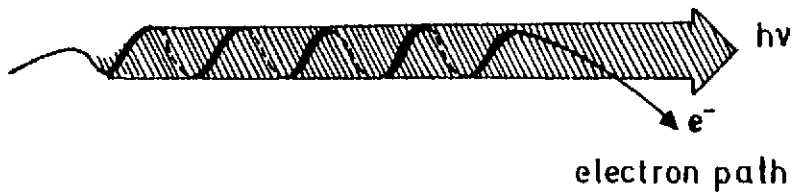


Fig. 4

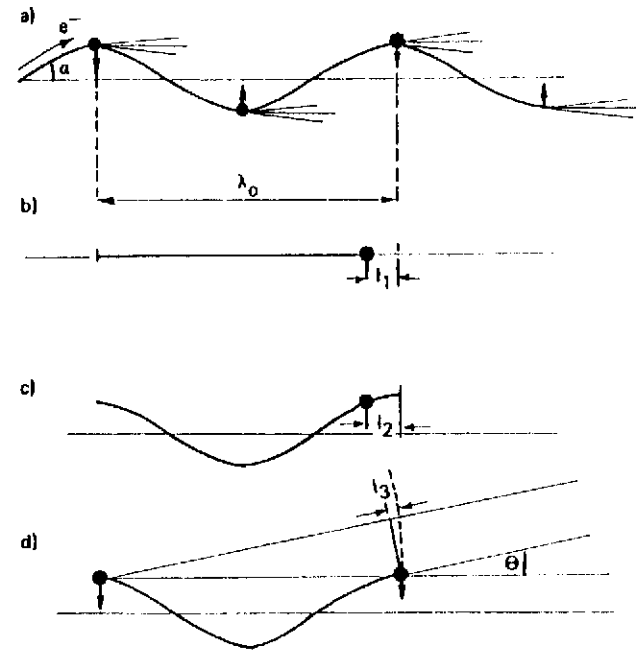


Fig. 5

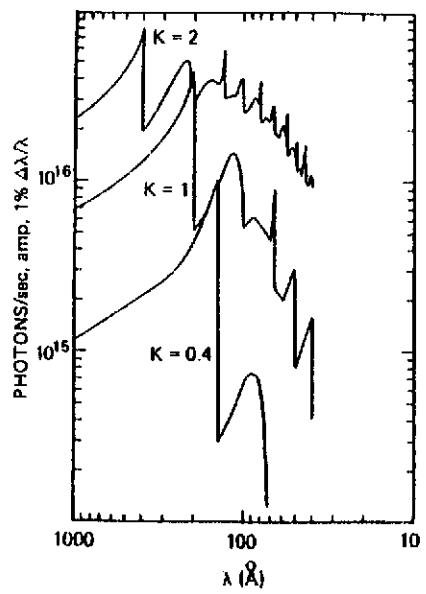


Fig. 6

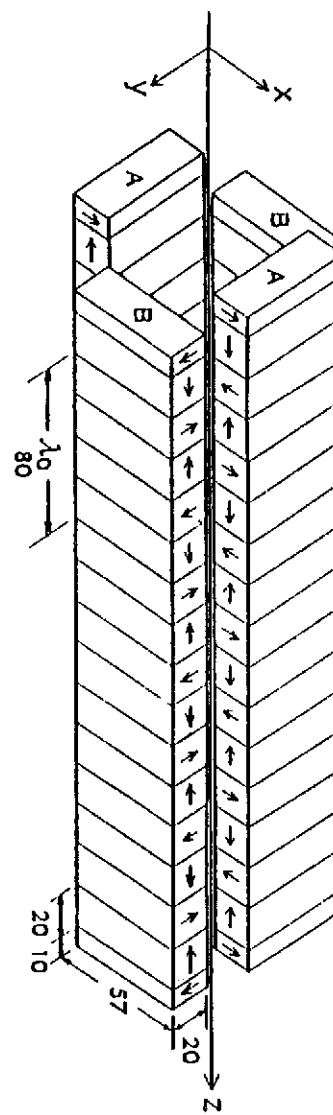


Fig. 7

a) Toroidal Holographic Grating Monochromator

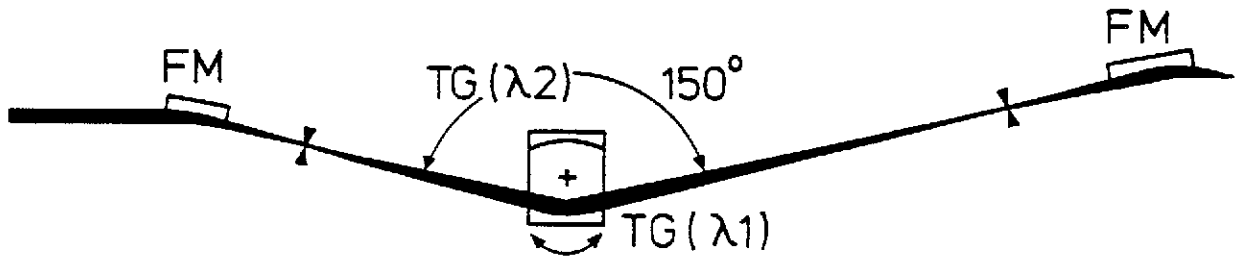


Fig. 8

FLIPPER BEAM-LINE

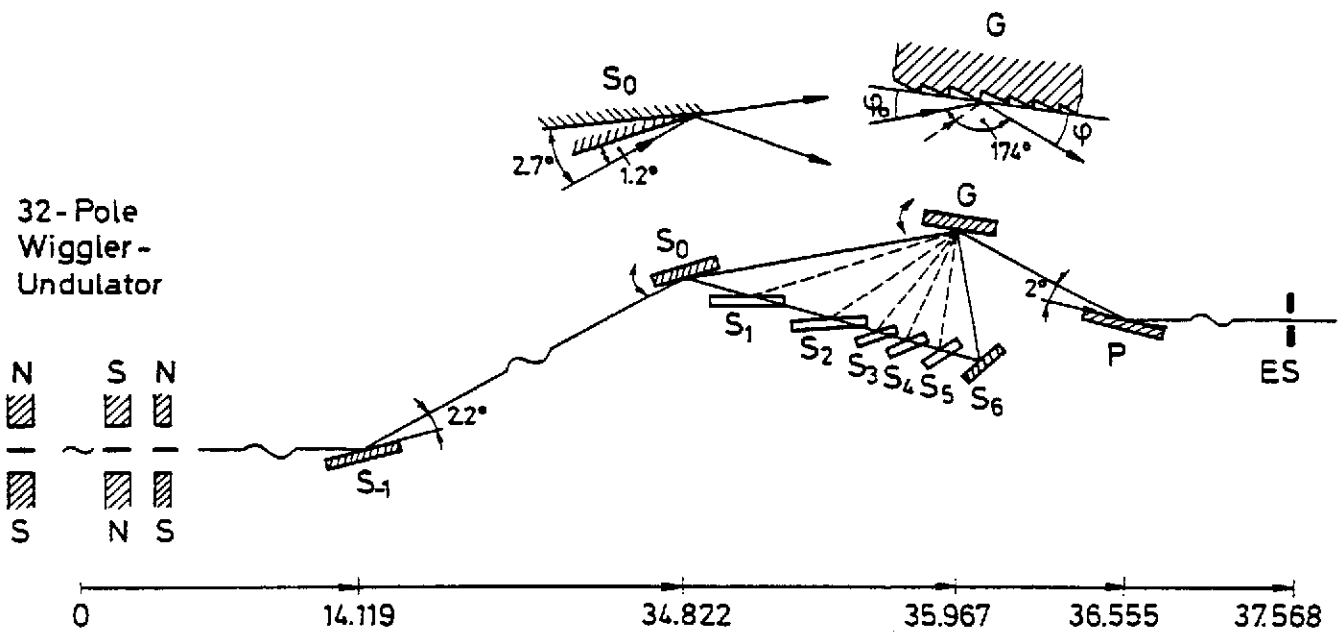


Fig. 9

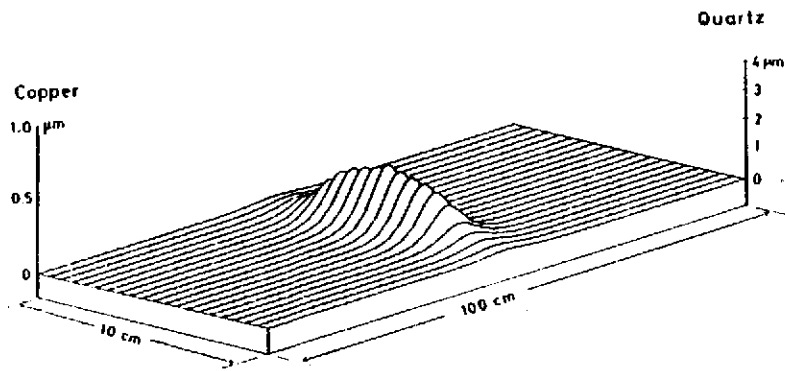


Fig. 10

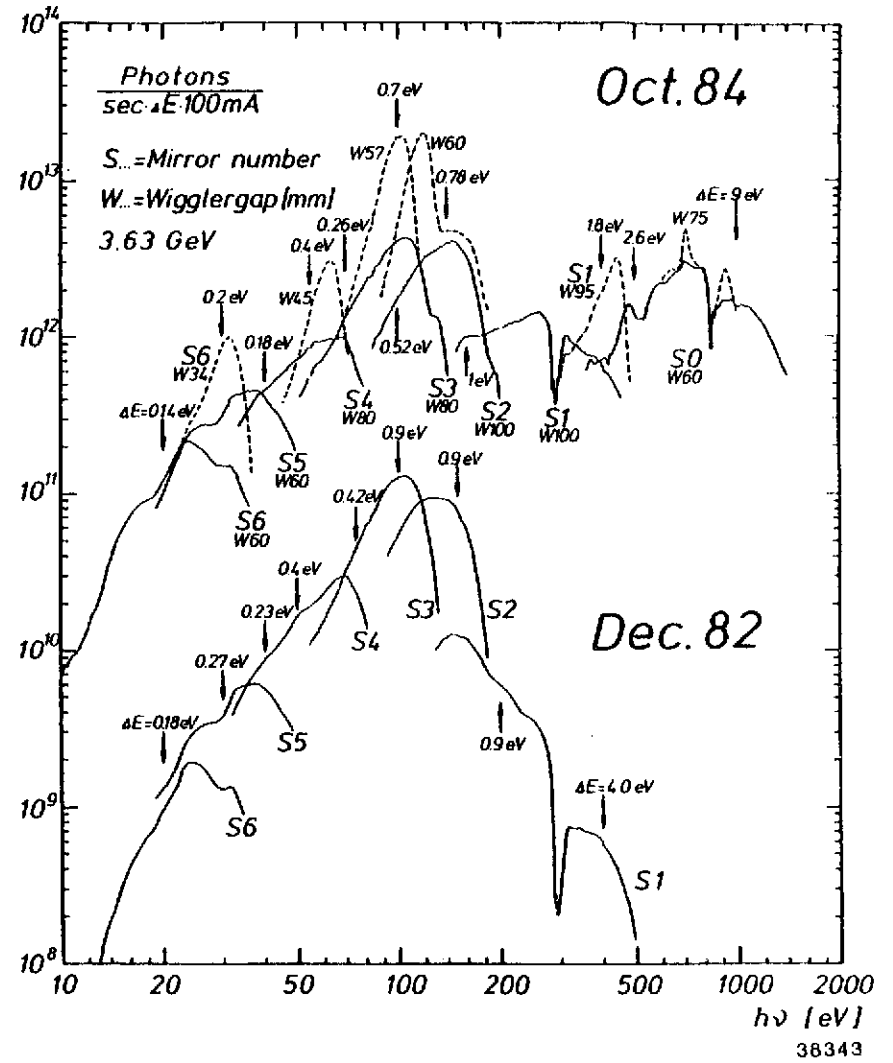


Fig. 11

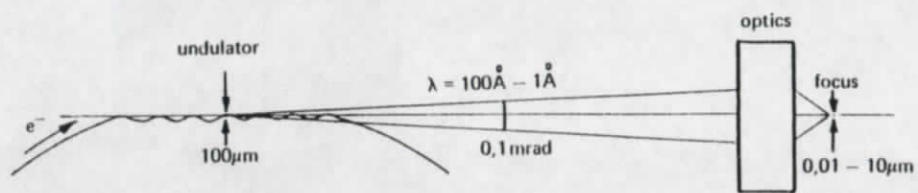


Fig. 12

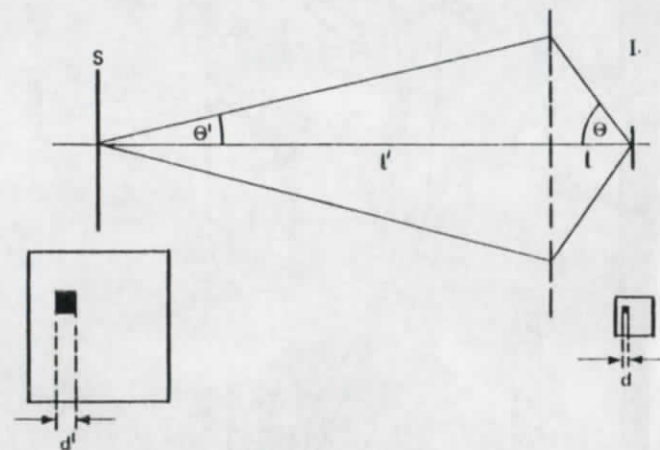


Fig. 13

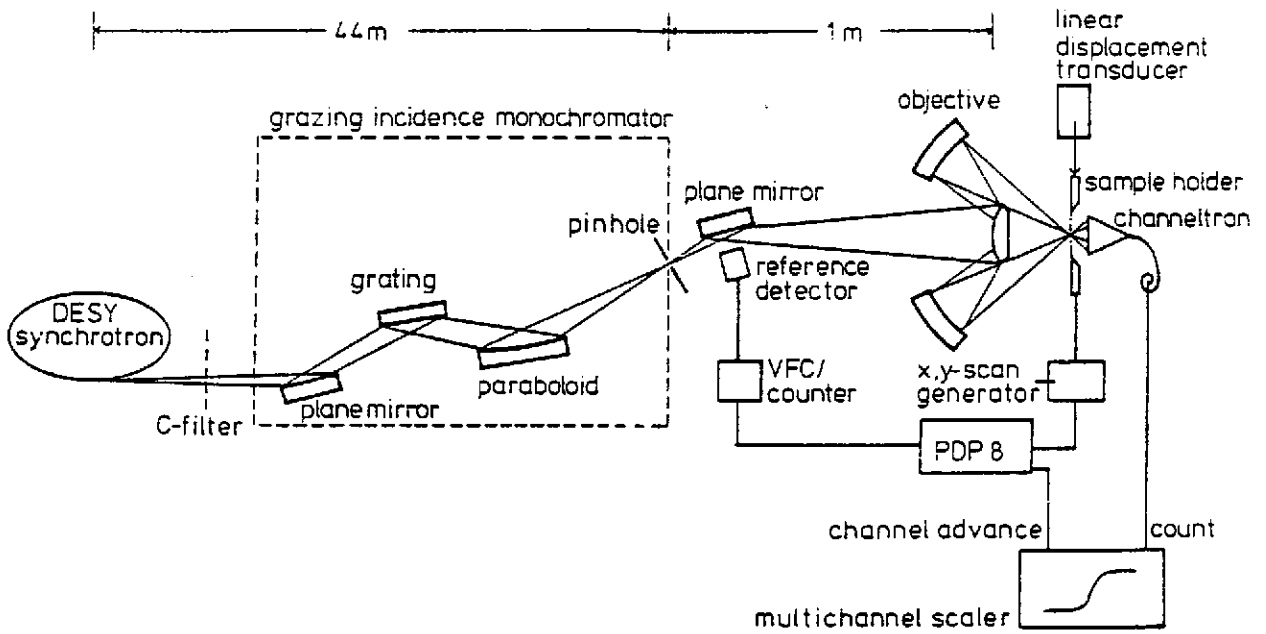


Fig. 15

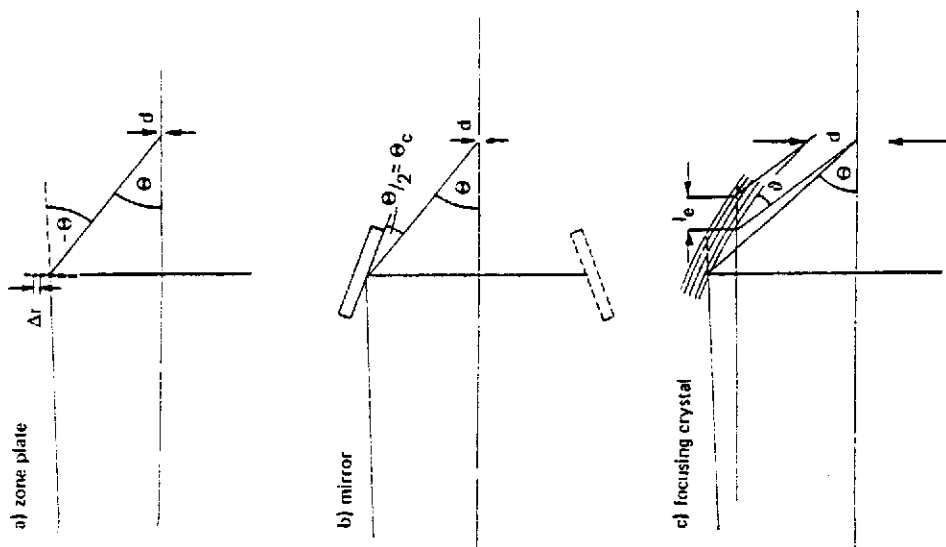


Fig. 16

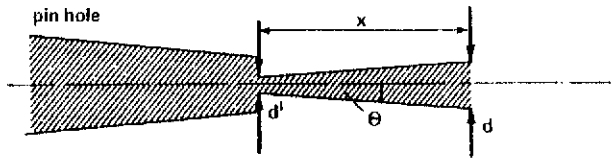


Fig. 16

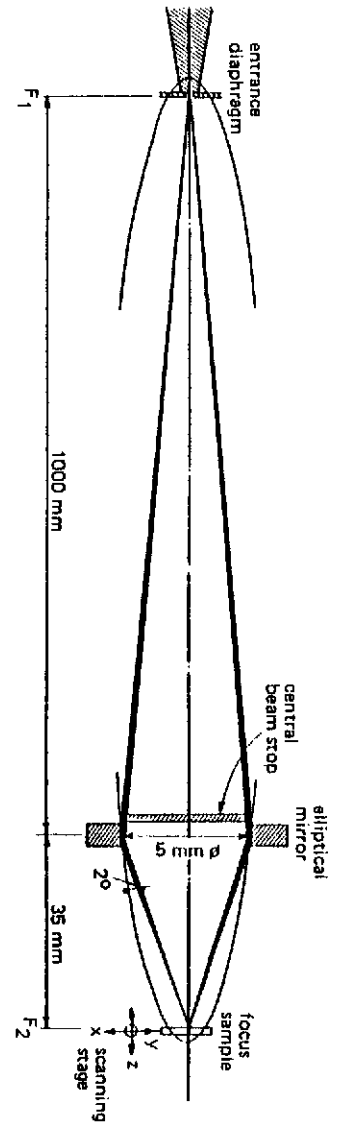


Fig. 17

